Study of angular cutting conditions using multiple scratch tests onto low carbon steel: An experimental-numerical approach

V. Seriacopi[a,b,*], S. Mezghani[c], S. Crequy[c], I.F. Machado[a], M. El Mansori[c], R.M. Souza[a]

[a] Surface Phenomena Laboratory, Escola Politécnica da Universidade de São Paulo, São Paulo, Brazil
[b] Federal Institute of São Paulo, Guarulhos, São Paulo, Brazil
[c] Laboratoire Mécanique, Surfaces, Matériaux et Procédés, Ecole Nationale Supérieure D'Arts et Metiers, Châlons-en-Champagne, France

ARTICLE INFO

Keywords:
Abrasion
Angular scratches
Low carbon steel
Cutting forces
Material removal
FEM

ABSTRACT

Multiple parallel scratches are often analyzed to understand the material removal mechanisms due to abrasion. However, successive scratches with different orientations may represent better the conditions found in machining processes, such as honing and belt finishing. The objective of this work was to analyze the cutting forces and the phenomena of material removal due to abrasion, arising from angular scratches in low carbon steel. Experimental and numerical techniques were considered. In both, analyses considered the presence of an initial set of parallel scratches, followed by a second set of scratches with different orientations (10, 20 or 30°) with respect to the previous one. The cutting action was performed by a tool representing an abrasive particle, which had a cono-spherical geometry with 235 μm tip radius and 30° apex angle. The cutting settings were: 50 m/min scratch velocity and 100 μm depth of cut. In the experimental part, scratches were conducted using a shaper machine tool equipped with a tungsten carbide (WC-Co) stylus. Tests were conducted on a Kistler platform, which allowed force measurement. Surfaces were later analyzed with an optical profilometer. The numerical simulations considered a ductile damage model with element deletion to provide the material removal during the scratches. Experimental and numerical results showed that the angle affects the cutting forces, especially when one scratch crosses a previously scratched region. The 20° case was the most critical, especially in terms of the cutting forces, due to the accentuated material strain-hardening for this condition. Likewise, this fact was corroborated by numerical results, which indicated a higher energy necessary to plastic deformation, and a reduced material removal at 20°.

1. Introduction

Abrasive wear remains as a key phenomenon in many practical applications, not only due to the significant amount of tribological damage that result from the action of hard particles, but also due to the constant need of improvement of manufacturing processes with cutting operations.

Abrasion studies are frequently conducted considering scratch tests, in which a single hard particle contacts a softer slab surface, promoting plastic deformation and/or material removal. The transition between the abrasive mechanisms during scratch tests was characterized and evaluated experimental and/or numerically, based on several approaches, considering: (i) mechanical properties (e.g. hardness, elastic modulus and hardness ratio, strain-hardening, interfacial shear strength) [1–5]; (ii) microstructural features (e.g. influence of the second phase particles, crystallographic orientation, deformation-induced phase transformation) [3,6–13]; (iii) material removal factor (f_{ab} – which relates the groove and pile-up areas), degree of wear and degree of penetration [8,14–16]; (iv) surface finishing (e.g. ground, mechanical and electrolytic polished surfaces) [17,18]; (v) relation between the normal load and geometric parameters of the scratch (e.g. scratch depth and width) [19,20]; (vi) effect of the attack angle of the abrasive particle on the apparent coefficient of friction [21–24]; and (vii) specific cutting energy modifications [25–27].

Additionally, a study related to the different orientations of the relative movement of an abrasive tool with respect to a ductile surface can be used to understand manufacturing by machining processes. This approach is based on the previous analyses conducted with multiple parallel scratches. Within this context, Williams and Xie investigated the interaction between parallel scratch tracks using an analytical model and experimental tests. These authors observed that the attack angle of the abrasive asperities played an important role to determine

* Corresponding author at: Surface Phenomena Laboratory, Escola Politécnica da Universidade de São Paulo, São Paulo, Brazil.
E-mail address: vanessaseriacopi@usp.br (V. Seriacopi).

https://doi.org/10.1016/j.wear.2019.01.101

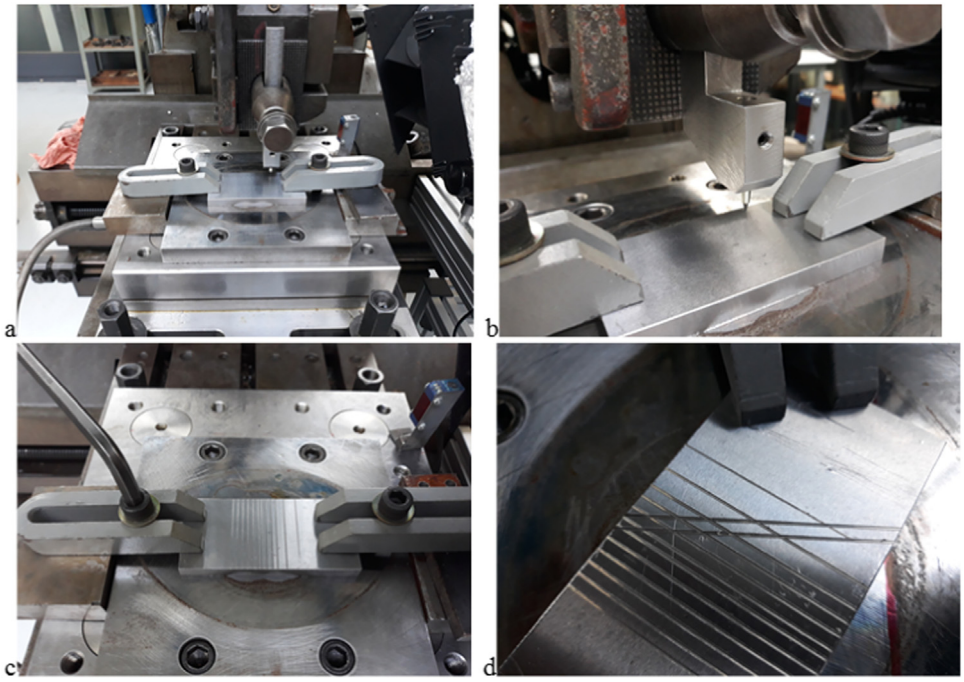

Fig. 1. Experimental setup of the scratch tests onto the 1020 steel conducted in the sequence a-d. Parallel scratches were carried out (a-c) and later a second set of parallel scratches was run at a specific angle (10, 20 or 30°) with respect to the previous one (d).

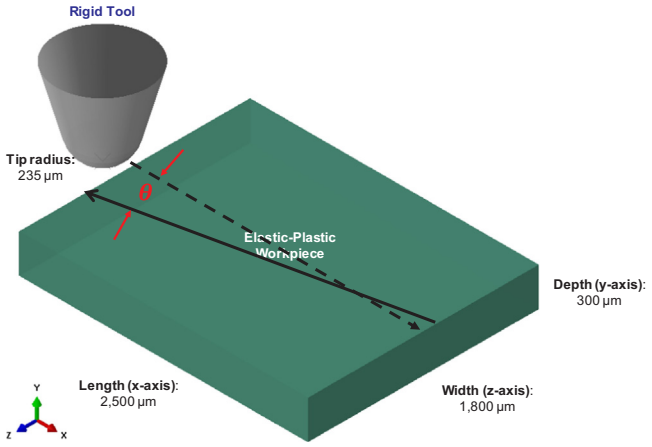

Fig. 2. Numerical modelling created to study the angled scratches. The following successive steps can be predicted here: (i-) first scratch due to the tool movement along x-direction; (ii-) tool moving along z-direction; and finally (iii-) angular scratches in the x-z plane (θ = 10, 20 and 30°), resulting in a V-shape or a X-shape depending on the angle and the consequent final scratch length.

Table 1
Johnson-Cook plasticity parameters of the AISI 1020 steel [36].

A [MPa]	B [MPa]	C	n	m	Tm [°C]	Tr [°C]	$\dot{\varepsilon}_0$ [s^{-1}]
213	53	0.055	0.345	0.81	1350	20	0.004

Table 2
Johnson-Cook ductile damage parameters of the AISI 1020 steel [37].

D_1	D_2	D_3	D_4	D_5
0.24	0.54	− 1.50	0	0

the deformation modes and micro-mechanisms (from ploughing to micromachining) on a flat surface [28]. In another work, the same authors identified that the abrasive geometry and the relative lateral displacement between repeated passes onto a copper specimen were prevailing to define the material removal rates. In that case, a map was created to design the dominant wear mechanism and wear rates. After multiple passes, material accumulation was observed, which provided the formation of wear debris [29]. Mezlini et al. carried out multiple scratches on aluminum alloys to reproduce repetitive loading conditions of granular materials. A microstructural characterization pointed out that the material removal mechanism by abrasion depends on the wedge interaction of the successive scratches. The subsurface strain-hardening was also included in the abrasion model for these materials, resulting in a better reproduction of the experimental results [30]. Focusing on ceramics and hard metals, Gee tested a scratch array varying the repetition number along the same scratch and using a normal load corresponding to 4 N (low load) with a diamond indenter. In this case, the parameter applied to evaluate the material removal was the scratch width. Furthermore, tangential force measurements, and the microstructural analyses, consisted of important resources to study the evolution of the multiple scratching features, allowing to detect the fracture with debris formation as a major cause of the damage on these materials [31]. Finally, Silva and Mello [32] used a high-resolution device to examine abrasion effects using superimposed scratches on a surface. The topographic and microstructural approaches allowed to identify the dominant abrasive mechanism. An experimental process simulation was specified according to positions of the parallel scratches, randomly distributed, creating patterns of surface morphology and topography, and considering constant and variable normal load conditions.

Table 3
Mechanical properties of the AISI 1020 steel [38].

Elastic modulus [GPa]	Poisson Ratio	Density [$kg.m^{-3}$]
200	0.30	7800

Based on this background of works focused on single scratch tests or multiple parallel scratches, the aim of this work consisted in analyzing the cutting forces and burr formation as a result of two consecutive scratches. However, different from previous works in the literature, the

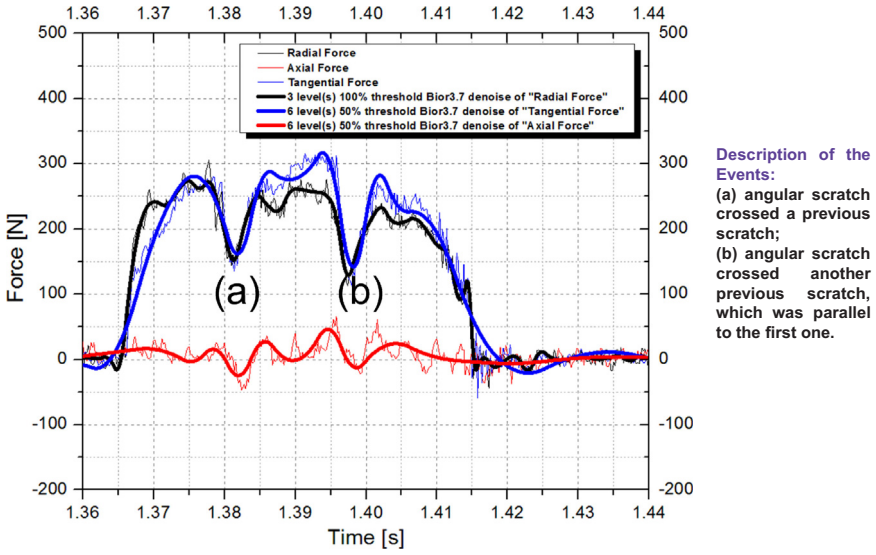

Fig. 3. Typical graph of the experimental cutting forces x time in the following conditions: without and with signal treatment (denoise). According to Fig. 1d, the angular scratch crossed some previous scratches. Thus, the points (a) and (b) show the influence of these events in the experimental cutting forces.

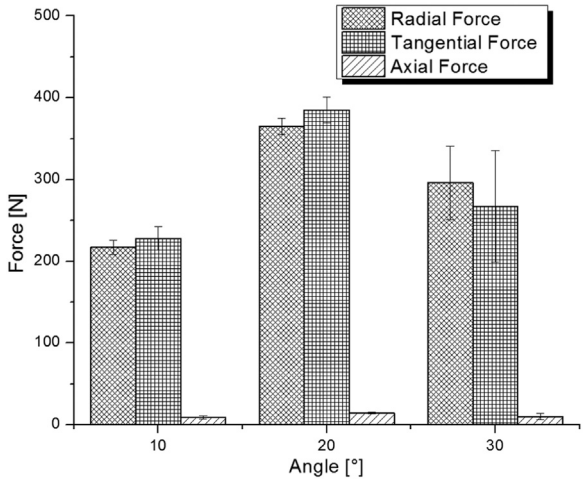

Fig. 4. Average experimental cutting forces obtained from the different angular scratch conditions.

Table 4
Experimental and numerical results of the tangential, axial and radial forces obtained from the angular scratches. Exp. = experimental, and Num. = numerical.

Condition	Tangential force [N]		Axial force [N]		Radial force [N]	
	Exp.	Num.	Exp.	Num.	Exp.	Num.
10°	228 ± 14	220.95	8.7 ± 1.8	7.20	217 ± 9	248.14
20°	385 ± 16	313.04	14.2 ± 1.3	13.13	365 ± 10	346.17
30°	267 ± 68	249.96	10 ± 4	8.42	296 ± 45	278.83

consecutive scratches were not parallel, but considered angles of 10, 20 or 30 degrees between them. Experimental and numerical procedures were developed to provide this evaluation, in which the axial, radial and tangential forces, as well as the material removal, were the outputs. Numerical analyses allowed to investigate and compare the material removal in the different conditions and were applied as a support to experimental evaluation.

2. Materials and methods

Angular scratches were conducted on a slab of low carbon steel, with hardness of 126 ± 6 HV_{30}. This carbon steel was selected for the analyses since single scratch tests in microscale were previously reported for other soft materials, including annealed AISI 1045 steel, and well-discussed in the literature. Pöhl, Hardes and Theisen [4] pointed out a more pronounced trend to micro-cutting on AISI 1045, in comparison with pure iron, due to its greater work hardening, which avoided a considerable pile-up formation.

In the present work, the abrasive tests were carried out using a modified shaper machine tool [33]. An initial set of parallel scratches was conducted on the slab, followed by a second set of scratches with different orientations (10, 20 or 30°) with respect to the previous one. The parameters of the test were: scratch velocity corresponding to 50 m min^{-1} and a constant depth of cut of 100 μm. The tool used to conduct scratch tests was made of cemented carbide (WC-Co), presenting a cono-spherical geometry with 233 ± 53 μm tip radius and 30° apex angle. Based on these settings, and considering the geometry of the tool, the slab material can be simplified as homogeneous. The experimental apparatus can be seen in Fig. 1. Five replicas for each condition (10, 20 and 30°) were tested to analyze the reproducibility and for comparison with the numerical approach.

The numerical model was prepared using the Finite Element Method (FEM) with Abaqus/Explicit® 2016 code. As displayed in Fig. 2, the tribosystem was modelled assuming that the tool was rigid, with a 235 μm tip radius, and the slab presented an elastic-plastic behavior. Johnson-Cook constitutive - Eq. (1) [34] - and ductile damage – Eq. (2) [35] - models were assigned to this slab to allow plastic deformation and material removal.

$$\bar{\sigma} = (A + B\varepsilon^{n})\left(1+C\ln\frac{\dot{\varepsilon}}{\dot{\varepsilon}_0}\right)\left[1-\left(\frac{T-T_r}{T_m-T_r}\right)^{m}\right] \quad (1)$$

Where: σ is the equivalent stress, ε is the equivalent plastic strain, $\dot{\varepsilon}$ is the strain rate, $\dot{\varepsilon}_0$ is the reference strain rate, A is the initial yield stress, B is the hardening modulus, C is the strain rate coefficient, n is the strain-hardening coefficient, m is the thermal softening coefficient, T is the process temperature, T_r is the room temperature and T_m is the melting temperature of the material [34].

$$\varepsilon^{f} = \left[D_1 + D_2 exp\left(D_3\frac{p}{q}\right)\right]\left[1+D_4\ln\frac{\dot{\varepsilon}}{\dot{\varepsilon}_0}\right]\left[1+D_5\left(\frac{T-T_r}{T_m-T_r}\right)\right] \quad (2)$$

Table 5
Scratch features calculated and normalized according with the schematic representation.

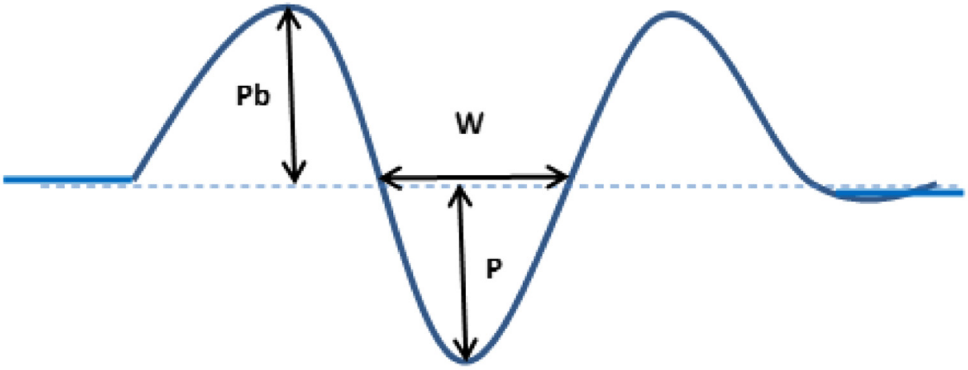

Parameters	Experimental	Numerical	Theoretical
Depth of penetration – P (mm)	0.12 ± 0.04	0.100	0.100
Width – W (mm)	0.49 ± 0.08	0.427	0.385
Pile-up height – P_b (mm)	0.07 ± 0.10	0.044 ± 0.003	-

In which: ε^f is the equivalent strain to failure, $D_1 - D_5$ are experimental failure constants of the Johnson-Cook damage equation, p is the pressure, q is the von Mises stress. The other parameters are described according to the terms in Eq. (1) [35].

The Johnson-Cook parameters of AISI 1020 steel used as modelling inputs are displayed in Table 1 [36] and Table 2 [37]. Furthermore, the other mechanical properties assigned to the carbon steel specimen are shown in Table 3 [38].

The finite element mesh assigned to the slab presented the following features: domain of 2500 × 1800 × 300 μm^3, discretized by 1,580,625 linear hexahedral elements of the C3D8 type. 32 CPUs available in high performance massively parallel machines of a cluster have been used for this modelling, resulting in approximately 18 h of computational time for each case of angular scratch. Regarding the boundary conditions, the numerical model was planned based on the following steps of the tool movement with respect to the slab:

(i) First scratch: the tool treads 3000 μm along the length (negative x-displacement - Fig. 2) with a constant depth of penetration of 100 μm (negative y-displacement - Fig. 2);
(ii) (ii-) Tool Moving: the tool goes through 650 μm along the width (negative z-displacement - Fig. 2);
(iii) (iii-) Angular scratches: the tool is moved back towards its origin, resulting in a second scratch, which considered the 10, 20 or 30° angle (x-z plane - Fig. 2). The results were evaluated in terms of cutting forces and burr formation. In this context, burr was defined as the chip formed at the intersection of two angular scratches.

During the experimental tests, a Kistler platform was mounted on the shaper machine tool and used to acquire the cutting forces (radial, axial and tangential forces). Moreover, the signal of the experimental cutting forces was treated using a signal denoiser. This noise filter was employed, consisting of an important resource to separate the wavelet and vibration effects. Additionally, after the scratch tests, the topography of the specimens was characterized using an optical profilometer to provide the information about the burr. Optical and scanning electron microscopy analyses were conducted on the cross sections at the intersection of consecutive scratches to investigate the influence of the abrasive mechanisms on the material subsurface.

3. Results and discussion

Fig. 3 presents an example of the experimentally calculated cutting forces as a function of time. When the tool crossed a previous scratch (groove) with a certain orientation, the cutting forces were reduced locally (points (a) and (b) in Fig. 3), as expected. In addition, Fig. 4 shows the average values of the experimental cutting forces, after the signal treatment. The lowest angle (10°) resulted in lower average values of the cutting forces.

Table 4 shows a comparison between experimental and numerical results of the cutting forces, indicating good agreement between numerical and experimental data. The differences are probably related to slight divergences in the mechanical properties and the approximated tool tip radius assumed in the modelling. Furthermore, despite several replacements of the tool, it could present wear caused by the successive scratches during the experimental tests, which was not considered in the numerical model.

Concerning the angular scratch features, the average width and pile-up height were characterized using optical profilometry. A theoretical analysis of the scratch width was conducted based on the literature [19]. These geometrical results are found in Table 5 and denote a good correlation of the numerical and experimental findings. Nevertheless, the difference in view of the pile-up height can be assigned to a slightly larger strain-hardening coefficient assumed in the FEM modelling, reducing the global plastic deformation when compared to the experimental one.

To evaluate the burr formation and its consequences in the manufacturing processes, two distinct analyses were conducted: (a)

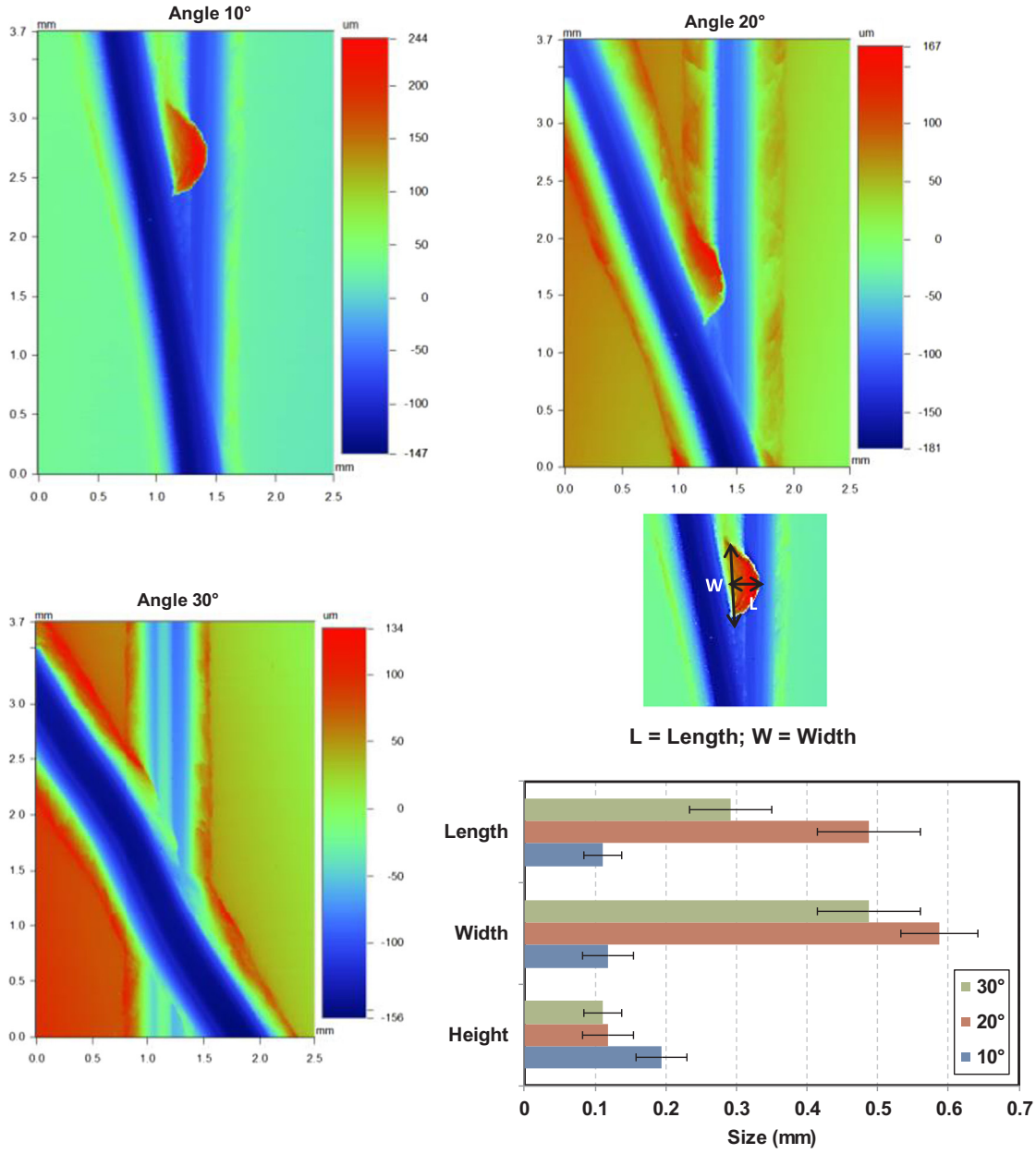

Fig. 5. Experimental results: topography characterization for all orientations. The burr features – length, width and height - are also displayed here.

experimental characterization of the topography, to verify the height effects (Fig. 5); and (b-) numerical result regarding the equivalent plastic strain at the nucleation of the damage, to observe the cumulative material (Fig. 6).

Figs. 5 and 6 show that the experimental burr formation was qualitatively reproduced by the numerical approach. The highest values of length and width occurred for the 20° orientation, which was also critical in terms of the cutting forces (Table 4). However, the burr height was more pronounced for the 10° orientation. Observing the experimental and numerical results, the following tendency can be reported: (i-) a large burr formation was found when the 10° angular scratch was conducted; (ii-) for the 20° condition, burr formation was accentuated, as well as pile-up occurrence; and (iii-) the burr was removed when the 30° scratch was conducted.

Considering that the modelling was validated, a numerical evaluation based on the material removal and dissipated energy during the cut can be used to understand the critical case corresponding to 20° scratch (cutting forces), and the burr formation (Figs. 5 and 6). Fig. 7 shows that the removed volume per distance decreased in the 10°–20° range, in which the plastic dissipation energy increases. This fact agrees with the higher cutting forces verified for the 20° condition (Table 4), i.e. the force should increase to provide the cutting with the occurrence of large plastic deformation of the carbon steel. Consequently, the lowest removed volume was observed in the 20° case (Fig. 7), in which a very high plastic dissipation energy was necessary to proceed the scratch, leading to a slight cutting energy (damage) decrease (Table 6).

Although lower than the 10° case, significant material removal is achieved for the 30° condition (Fig. 7) because of the aggressive scratch setup. The geometrical settings lead to a large amount of energy dissipated due to the damage (cutting energy in Table 4), in conjunction with a reduction of the plastic dissipation energy.

Fig. 8**(a-d)** present the characterization of the cross sections at the intersection of two angled scratches obtained experimentally (section indicated in Fig. 9**a**). The observation of the etched material subsurface using optical microscopy (Fig. 8**a**) allowed verifying the presence of a deformed layer, whose thickness is dependent on the angle between

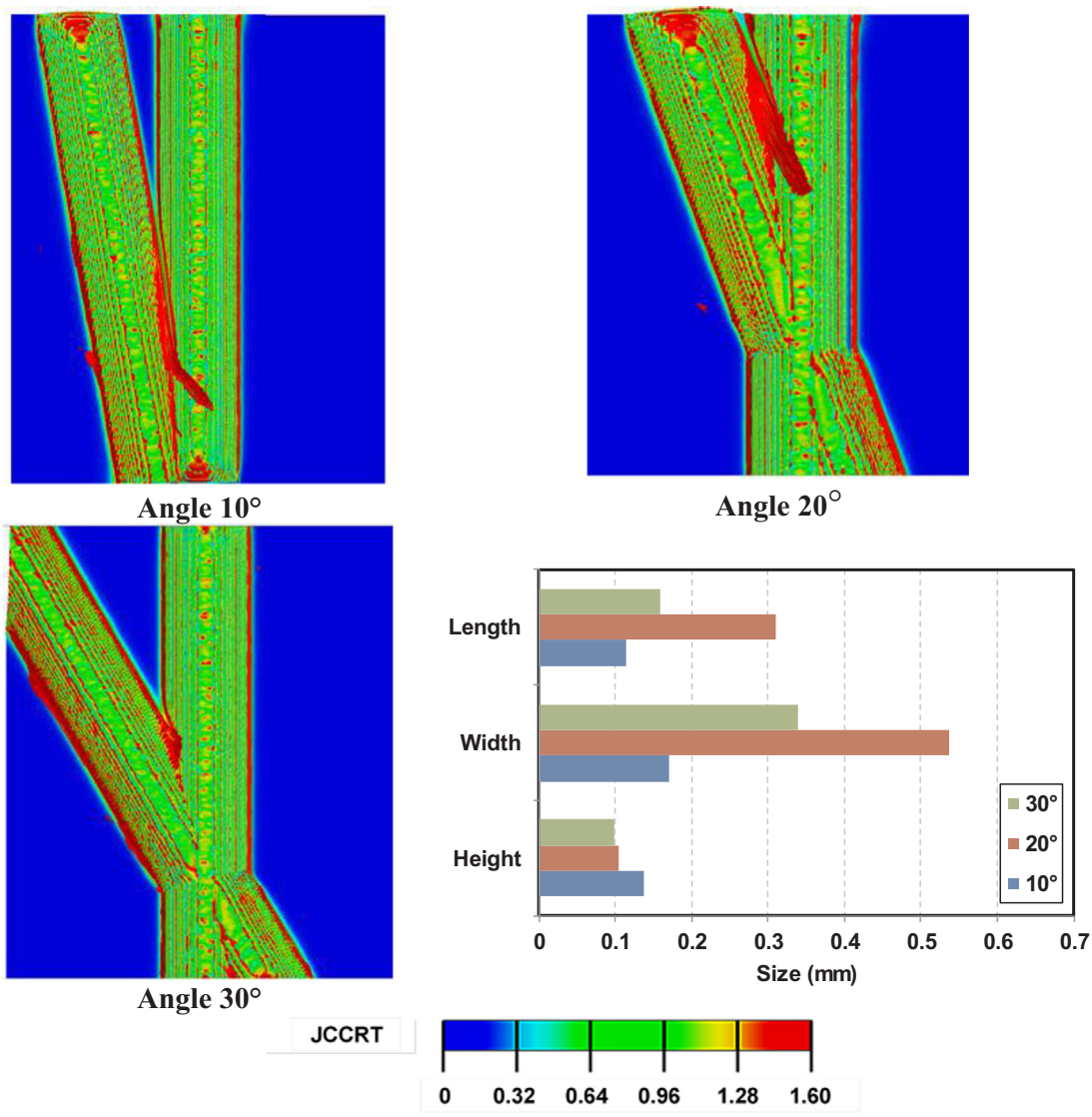

Fig. 6. Numerical results: Equivalent plastic strain at the onset of the fracture, defined by the Johnson-Cook damage criterion (JCCRT) for all orientations. The burr features – length, width and height – obtained from the numerical analyses are available here.

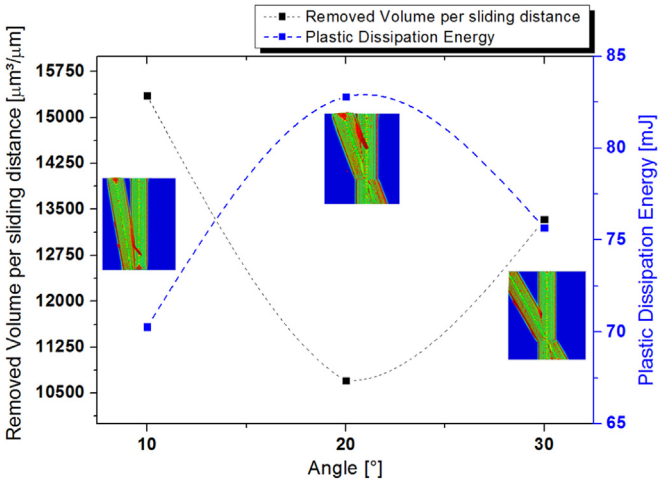

Fig. 7. Numerical results of the material removal and plastic dissipation energy as a function of the orientation of the angular scratch.

scratches. This characterization shows that the thinnest deformed layer was observed at 20°, which indicated a higher material hardening and a reduced removed volume in this case. SEM images in Fig. 8**(b-c)** provide more details of the deformed layers obtained in each case. The mean values and standard deviations of five representative measurements resulting from this experimental procedure are also provided (Table 7). The thickness of the deformed layer is in agreement with the behavior of the cutting forces (Table 4):

(i) 10° case (Fig. 8**b**) – maximum deformed layer thickness could be associated with the minimum forces necessary to cut the carbon steel. For this geometrical setup, the material strain-hardening was not favored during the combination of scratches, resulting in an intensified removed volume with massive plastic deformation (Fig. 7);

(ii) 20° case (Fig. 8**c**) - minimum deformed layer thickness corresponded to the maximum cutting forces, which corroborated the hypothesis of material strain-hardening with the lowest material removal (Fig. 7);

(iii) 30° case (Fig. 8**d**) – consisted of an intermediary condition between 10° and 20° responses. The deformed layer thickness was within the range determined by the lower limit (20°) and the higher limit

on the scratch crossing,

Table 6
Numerical results in terms of some parcels of the dissipated energy during the cutting.

Condition	Plastic dissipation energy [mJ]	Cutting energy [mJ]
10°	70.28	1.06
20°	82.79	0.86
30°	75.65	0.92

(10°). Conversely, the opposite could be thought based on the cutting forces. Therefore, as expected, an intermediate value of the removed volume was predicted by FEM for the 30° angle case (Fig. 7).

Fig. 9 presents a numerical analysis of the plastic strain fields at the material subsurface, indicating the section at which the experimental and numerical analyses were effected (Fig. 9**a**). For all angles, the equivalent plastic strain decreased from the surface to the subsurface reaching a minimum value of 0.009. Moreover, the numerical thickness of the deformed layer followed the experimental behavior (Table 7), i.e. the scratches at 30° resulted in thicknesses lower than those at 10° and higher than those at 20°. A result similar to the 20° critical case was found by Mezlini et al. [30] for parallel scratch tests conducted onto an annealed aluminum alloy. Those authors observed that a significant subsurface strain-hardened layer was formed in addition to an accumulation of deformed material on the scratch sides as a function of the alloy ductile properties. Therefore, the experimental-numerical results of the 20° case could be explained using two approaches:

(a) mechanical properties - subsurface layer analyses (Table 7) denote the material strain-hardening influence;
(b) damage properties - the higher values related to burr length and width (Figs. 5 and 6) imply in a greater material plastic deformation due to material ductile behavior.

4. Conclusions

The experimental and numerical studies developed in this work, to analyze angular scratches (10, 20 and 30°) on low carbon steel, provide the following conclusions:

- The numerical model was able to reproduce the experimental scratch features, cutting forces and deformed layer thickness formed on the carbon steel, for all angular scratches evaluated in this work;
- Cutting forces, burr formation and subsurface deformed layer values indicated that the 20° case was the most critical. The material strain-hardening was more accentuated when a 20° angle was used. This outcome is corroborated with a higher plastic dissipation energy as well as a lower removed volume for the 20° condition, when compared to the others;
- Conversely, considering minimum and maximum scratch angles (10° and 30°), it was noticed that the cutting forces showed the trend to decrease for 10°. Moreover, the plastic dissipation energy and removed material analyses indicated 30° case as an intermediary condition between 10° and 20° angular scratches, which agrees with the deformed layer thickness evaluation (material mechanical properties) and burr removal (ductile damage).

As a final remark, it can be said that the approach implemented here is of technological importance to design and reproduce surfaces manufactured by machining processes. The numerical procedure and the experimental characterizations and measurements are essential to understand the machined surface and to design processes for its modification.

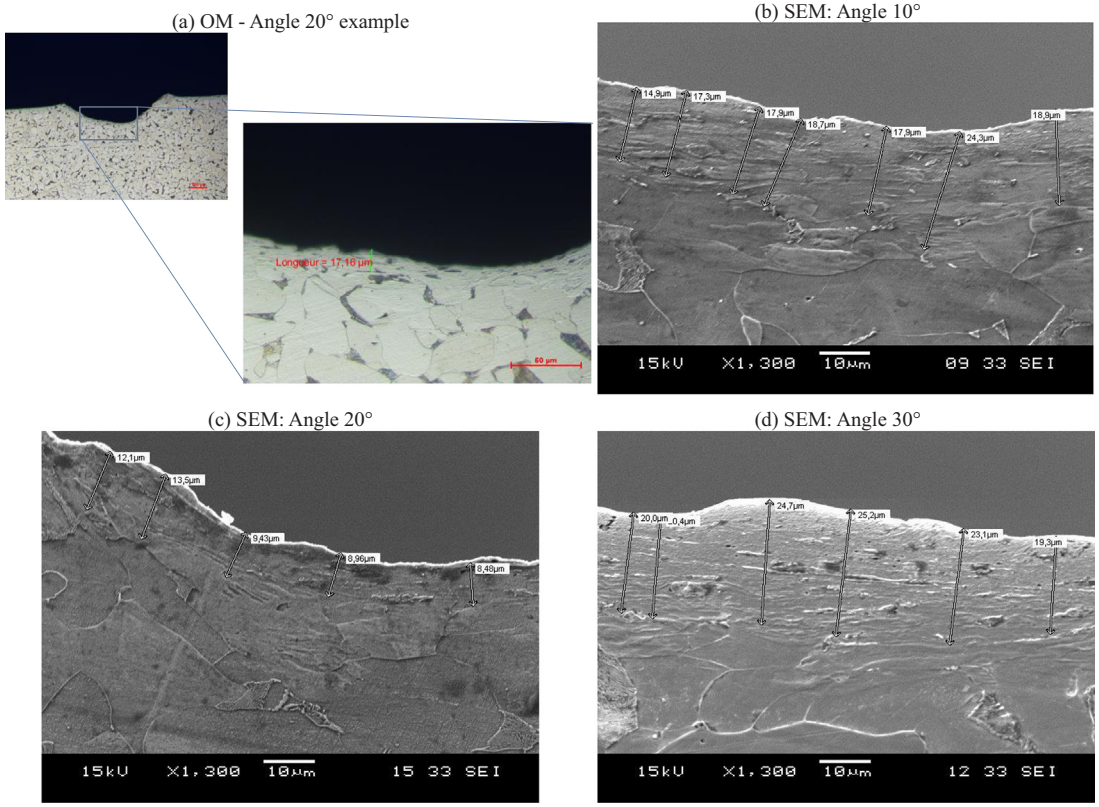

Fig. 8. Characterization by optical and scanning electron microscopies (OM and SEM) of the cross sections at the intersection of two consecutive scratches with different orientations onto the AISI 1020 steel: (a) OM – example for angle 20°; SEM - (b) angle 10°, (c) angle 20°; and (d) angle 30°.

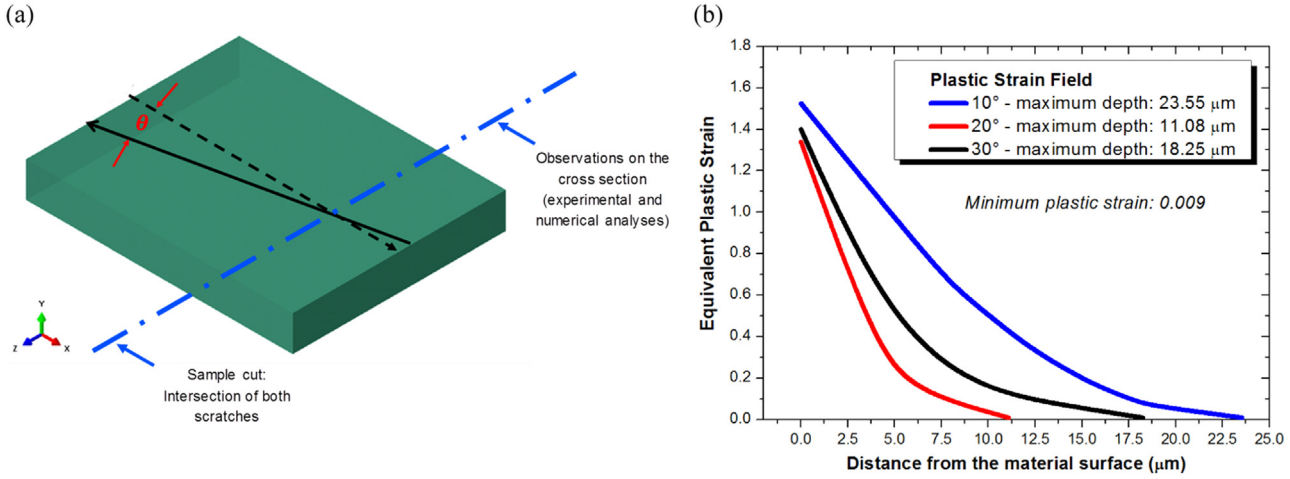

Fig. 9. Indication of the cross section evaluated throughout numerical and experimental characterizations (a). In addition, the equivalent plastic strain, obtained from the numerical simulation, is shown along the subsurface layer of the material (b).

Table 7
Summary of the deformed layer thickness (experimental and numerical results) to promote an overall comparison.

Angle (°)	Thickness of the deformed layer - Experimental	Thickness of the deformed layer - Numerical
10	22.5 ± 2.6	23.55
20	10.5 ± 2.2	11.08
30	17.3 ± 1.5	18.25

Acknowledgments

The authors would like to acknowledge the Brazilian research support agencies: Sao Paulo Research Foundation (FAPESP) Grant number 2016/18014-6, National Council for Scientific and Technological Development (CNPq), and Foundation for the Support of University of Sao Paulo (FUSP).

References

[1] K. Hokkirigawa, K. Kato, An experimental and theoretical investigation of ploughing, cutting and wedge formation during abrasive wear, Tribol. Int. 21 (1988) 51–57.
[2] K. Hokkirigawa, K. Kato, Z.Z. Li, The effect of hardness on the transition of the abrasive wear mechanism of steels, Wear 123 (1988) 241–251.
[3] P.C. Machado, J.I. Pereira, J.J. Penagos, A. Sinatora, The effect of in-service work hardening and crystallographic orientation on the micro-scratch wear analysis of Hadfield steel, Wear 101 (2017) 1064–1073.
[4] F. Pöhl, C. Hardes, W. Theisen, Scratch behavior of soft metallic materials, AIMS Mater. Sci. 3 (2016) 390–403.
[5] F. Pöhl, S. Schwarz, P. Junker, K. Hackl, W. Theisen, Indentation and scratch testing – experiment and simulation, Int. Conf. Stone Concr. Mach. 3 (2015) 292–308.
[6] V. Seriacopi, Evaluation of Abrasive Mechanisms in Metallic Alloys during Scratch Tests: A Numerical-Experimental Study in Micro-scale (Ph.D. thesis), Univeristy of Sao Paulo, Sao Paulo, Brazil., 2017.
[7] L.A. Franco, Abrasion of Gray Cast Iron: Application to Automotive Engines(Ph.D. thesis), Univeristy of Sao Paulo (In portuguese), 2015.
[8] K.-H. Zum Gahr, Wear by hard particles, Tribol. Int. 31 (1998) 587–596, https://doi.org/10.1016/S0301-679X(98)00079-6.
[9] Zum Gahr, Microstructure and wear of materials, Tribol. Ser. (1987) 10.
[10] J. Hu, D.Y. Li, R. Llewellyn, Synergistic effects of microstructure and abrasion condition on abrasive wear of composites — a modeling study, Wear 263 (2007) 218–227.
[11] F. Pöhl, A. Mohr, W. Theisen, Effect of matrix and hard phase properties on the scratch and compound behavior of wear resistant metallic materials containing coarse hard phases, Wear 376–377 (2017) 947–957.
[12] M.B. Tkaya, S. Mezlini, M. El Mansori, H. Zahouani, On some tribological effects of graphite nodules in wear mechanism of SG cast iron: finite element and experimental analysis, Wear 267 (2009) 535–539.
[13] M. Mendas, S. Benayoun, Investigating the effects of microstructure on the wear mechanisms in lamellar cast irons via microscratch tests, Tribol. Int. 67 (2013) 124–131, https://doi.org/10.1016/j.triboint.2013.07.009.
[14] L.A. Franco, A. Sinatora, Material removal factor (f ab): a critical assessment of its role in theoretical and practical approaches to abrasive wear of ductile materials, Wear 382–383 (2017) 51–61.
[15] T. Kayaba, K. Hokkirigawa, K. Kato, Analysis of the abrasive wear mechanism by successive observations of wear processes in a scanning electron microscope, Wear 110 (1986) 419–430.
[16] G. Goel, H.P. Cherukuri, A. Toro, A numerical study of abrasive wear in tillage tools due to soil-tool interaction, Simulia, Rhode Isl. Conv. (2012) 1–11.
[17] V. Seriacopi, N.K. Fukumasu, R.M. Souza, I.F. Machado, Analysis of abrasion mechanisms in the AISI 303 stainless steel: effect of deformed layer, Procedia CIRP 45 (2016) 187–190.
[18] H.S. Avery, Work hardening in relation to abrasion resistance, Climax Molybd. Compil. (1974) 43–77.
[19] R.L. Kobrick, D.M. Klaus, K.W. Street, Developing abrasion test standards for evaluating lunar construction materials, SAE Int. J. Aerosp. 4 (2009) 2009–01-2377, https://doi.org/10.4271/2009-01-2377.
[20] R.L. Kobrick, D.M. Klaus, K.W. Street, Standardization of a volumetric displacement measurement for two-body abrasion scratch test data analysis, Wear 270 (2011) 650–657, https://doi.org/10.1016/j.wear.2011.01.026.
[21] S. Mezlini, M. Zidi, H. Arfa, M.B. Tkaya, P. Kapsa, Experimental, numerical and analytical studies of abrasive wear: correlation between wear mechanisms and friction coefficient, Comptes Rendus Mécanique 333 (2005) 830–837.
[22] M.B. Tkaya, M. Zidi, S. Mezlini, H. Zahouani, P. Kapsa, Influence of the attack angle on the scratch testing of an aluminium alloy by cones: Experimental and numerical studies, Mater. Des. 29 (2008) 98–104.
[23] M.B. Tkaya, H. Zahouani, S. Mezlini, P. Kapsa, M. Zidi, A. Dogui, The effect of damage in the numerical simulation of a scratch test, Wear 263 (2007) 1533–1539.
[24] F. Wredenberg, P.-L. Larsson, On the numerics and correlation of scratch testing, J. Mech. Mater. Struct. 2 (2007) 573–594.
[25] H. Wang, H.-.T. Lin, A.A. Wereszczak, N. Yang, J.A. Jensen Specific energy and scratch hardness of gamma titanium aluminides subjected to single-grit pendulum scratching, in: Proceedings of the ASME International Combustion Engine Division 2006 Fall Technnology Conference, 2006,p. 437–448.
[26] J.M. Vélez, D.K. Tanaka, A. Sinatora, A.P. Tschiptschin, Evaluation of abrasive wear of ductile cast iron in a single pass pendulum device, Wear 250–251 (2001) 1315–1319, https://doi.org/10.1016/S0043-1648(01)00760-8.
[27] J. Lee, Experimental Investigation of the Bore Honing Process.Pdf, Trans. ASME (1993) 115, https://doi.org/10.1115/1.2901783.
[28] J.A. Williams, Y. Xie, The generation of wear surfaces by the interaction of parallel grooves, Wear 155 (1992) 363–379, https://doi.org/10.1016/0043-1648(92)90095-P.
[29] Y. Xie, J.A. Williams, The generation of worn surfaces by the repeated interaction of parallel grooves, Wear 162–164 (1993) 864–872.
[30] S. Mezlini, P. Kapsa, C. Henon, J. Guillemenet, Abrasion of aluminium alloy: effect of subsurface hardness and scratch interaction simulation, Wear 257 (2004) 892–900, https://doi.org/10.1016/j.wear.2004.05.004.
[31] M.G. Gee, Low load multiple scratch tests of ceramics and hard metals, Wear 250–251 (2001) 264–281, https://doi.org/10.1016/S0043-1648(01)00591-9.
[32] W.M. da Silva, J.D.B. de Mello, Using parallel scratches to simulate abrasive wear, Wear 267 (2009) 1987–1997.
[33] J. Xu, M. El Mansori, Wear characteristics of polycrystalline diamond tools in orthogonal cutting of CFRP/Ti stacks, Wear 376–377 (2017) 91–106, https://doi.org/10.1016/j.wear.2016.11.038.
[34] G.R. Johnson, W.H. Cook A constitutive model and data for metals subjected to large strains, high strain rates and high temperatures. in: Proceedings of the 7th International Symposium on Ballistics, vol. 21, 1983,p. 541–547.
[35] G.R. Johnson, W.H. Cook, Fracture characteristics of three metals subjected to various strains, strain rates, temperatures and pressures, Eng. Fract. Mech. 21 (1985) 31–48.

[36] C.F. Kui, L.Y. Fei, X.J. Xue, H.K. Peng, X.K. Ge, W. Yu, et al., The dynamic characteristics and constitutive model of 1020 steel, Emerg. Mater. Res. 6 (2017) 124–131, https://doi.org/10.1680/jemmr.16.00019.
[37] R. Kupchella, D. Stowe, X. Xiao, A. Algoso, J. Cogar, Incorporation of material variability in the Johnson Cook model, Procedia Eng. 103 (2015) 318–325, https://doi.org/10.1016/j.proeng.2015.04.053.
[38] ASM International, ASM Handbook, Volume 1: Properties and Selection: Irons, Steels, and High-Performance Alloys, ASM International, USA, 1990.